08,02,04

Electron Transport in Strontium Iridate Thin Films and Superconducting Heterostructures

© Yu.V. Kislinskii[1], I.E. Moskal[1], V.A. Baydikova[1,2], K.Y. Constatinian[1], N.V. Dubitskiy[1,3], A.M. Petrzhik[1], G.D. Ulev[1,3], A.V. Shadrin[1,4], V.A. Shmakov[1], G.A. Ovsyannikov[1]

[1] Kotelnikov Institute of Radio Engineering and Electronics, Russian Academy of Sciences, Moscow, Russia
[2] MIREA — Russian Technological University, Moscow, Russia
[3] National Research University Higher School of Economics, Moscow, Russia
[4] Moscow Institute of Physics and Technology (National Research University), Dolgoprudny, Moscow Region, Russia

E-mail: yulii@hitech.cplire.ru

Received March 6, 2025
Revised March 6, 2025
Accepted May 5, 2025

Thin films of strontium iridate that have a feature of strong spin-orbit coupling were made. They were deposited by three technological procedures which are direct current sputtering, pulsed voltage source sputtering, laser ablation. By electrical resistivity versus temperature dependencies the mechanisms of charge carrier transport were determined for the films. A superconducting current transport models for junctions which based on cuprate $YBa_2Cu_3O_{7-x}$ and niobium which are separated by strontium iridate barriers were proposed.

Keywords: strontium iridate, hopping conductivity, spin-orbit coupling, electron-electron interaction, Josephson effect.

DOI: 10.61011/PSS.2025.07.61895.24HH-25

1. Introduction

Development of Josephson junctions, where spin-dependent processes play a major role, captures heightened attention [1,2]. In particular, it was shown theoretically that spin-orbit interaction (SOI) causes generation of spin-triplet superconducting current [3–6]. Layers of Pt (metal with high atomic weight) were included into a ferromagnetic layer to study the SOI effect at the properties of Nb/Pt/Co-Ru/Pt/Nb contacts. Specific voltages of the produced contacts were around 1 nV [7].

Recently the contacts of oxide superconductor with strontium iridates (SI) — materials of the Ruddlesden-Popper series $Sr_{n+1}Ir_nO_{3n+1}$, having strong SOI [8] and causing the formation of non-trivial surface states, are drawing the heightened interest [9]. In the experiment it manifests by the occurrence of the conductivity peak at zero voltage [10], by the difference of the superconducting current-phase dependence on the sinusoidal one [10,11]. In the composite Josephson contacts based on cuprate superconductor $YBa_2Cu_3O_{7-x}$ with a layer of iridate and a top superconducting layer from Nb, the role of strontium iridate is critical, which at $n = 1$ (Sr_2IrO_4) is a canted antiferromagnetic with magnetization of $\sim 10^{-2}\,\mu$B/atom Ir, and at $n = \infty$ ($SrIrO_3$) — a paramagnetic metal. As a result of this the electrophysical characteristics of the contacts with different SI layers turn out to be significantly different. Current-voltage curves (CVCs) of the structures with the layers from dielectric Sr_2IrO_4 demonstrated the Fiske steps [12] and the tunnel feature of gap Nb [10], which means the presence of the tunnel transport of Cooper pairs therein. Contacts with layers of $SrIrO_3$ had much lower resistivities R_NA (R_N and A are the normal resistance and the area of the junction correspondingly), which is inherent in the Josephson contacts with the direct conductivity [13]. According to the data on resistivities of $SrIrO_3$ and Sr_2IrO_4 films [13,14], their use as layers in Josephson junctions with the basic superconducting electrode from cuprate superconductor $YBa_2Cu_3O_{7-x}$ should show in the differences of specific voltages I_CR_N (I_C — critical current). In the experiment these voltages were $I_CR_N \approx 50\,\mu$V for Sr_2IrO_4 barriers, and $I_CR_N \approx 0.5\,\mu$V in the case of $SrIrO_3$ layers. This paper will provide data on the electron transport characteristics of the SI layers. Comparison of CVCs of Josephson junctions with the layers from different iridates and corresponding dependences of the critical current on the magnetic field has not been previously discussed in the literature and is mentioned in this report for the first time.

2. Experimental procedure

Thin $SrIrO_3$ films were applied by the methods of laser ablation and pulse cathode sputtering onto different substrates from (001) $(LaAlO_3)_{0.3}(Sr_2TaAlO_6)_{0.7}$ — (LSAT), (001) $LaAlO_3$ — (LAO) and (110) $NdGaO_3$

(NGO). The a-parameter of $SrIrO_3$, which is the primary one for epitaxy and is equal to 0.396 nm, is higher than the a-parameters of the substrates: 0.387 nm LSAT, 0.385 nm NGO, 0.379 nm LAO. Therefore, the $SrIrO_3$ lattice was exposed to compression, which increases the resistivities of films [15]. In mesa-heterostructures (MHS) the layer films were sputtered on the superconducting cuprate $YBa_2Cu_3O_7$ with a-parameter of 0.386 nm. The epitaxy conditions in sputtering of layers in MHS are close to the conditions of sputtering onto NGO substrates. Parameters of impulse cathode sputtering of $SrIrO_3$ on these substrates were the following: temperature $T = 770\,^{\circ}\mathrm{C}$, total pressure 0.25 mBar, ratio of flows of Ar and O_2 1 : 3.5, sputtering speed of 10 nm per hour. For dielectric Sr_2IrO_4 a-parameter is 0.55 nm [16], which in epitaxy at 45 degrees to the substrate lattice yields the effective parameter of $a/2^{1/2} = 0.389$ nm. Usually, to sputter iridates, $SrTiO_3$ substrates are used with a-parameter of 0.391 nm, which provides the least mismatch of a-parameters. Sr_2IrO films were sputtered both by an excimer laser at $T = 780\,^{\circ}\mathrm{C}$ and pressure of O_2 0.5 mBar, and by impulse cathode sputtering at $T = 820\,^{\circ}\mathrm{C}$, pressure of Ar 0.5 mBar.

After geometry formation [10] the critical temperature of MHS was determined by Nb film and made $T_C = 8.4$ K, which was much lower than the critical temperature of $YBa_2Cu_3O_{7-x}$ $T_C = 61$ K [11]. Electric transport measurements of thin films are done using a four-point layout with the upper limit of resistance measurement of around 5 GΩ, which at thicknesses of films of around 20 nm yielded maximum values of resistivities $\rho \sim 10^4\,\Omega\,\mathrm{cm}$ or minimum values of $\sigma = 1/\rho \sim 10^{-4}\,(\Omega\,\mathrm{cm})^{-1}$. CVC measurements in MHS with layers of iridates were carried out in the Set-up with the current noise of around 2 μA, which yielded the minimum value of the found critical current of around 0.5 μA [10].

3. Results of electrical measurements of thin films

Resistances of $SrIrO_3$ films were measured from room temperature to 4 K at direct current. Temperature dependences of resistivities $\sigma = 1/(R \cdot t)$, where R — resistance, and t — film thickness, are shown in Figure 1.

The general feature of these dependences is that σ increases as the temperature increases from 20 to 200 K. Samples sputtered onto LSAT and LAO substrates had resistivities in the room of 0.5 mΩ cm and 1.3 mΩ cm accordingly, and the film sputtered onto NGO — around 3 mΩ cm. Maximum resistance of metal — Mott–Regel limit at electron-electron interaction therein is around $\rho \sim 10$ mΩcm [17], which is higher than in the studied samples. In the model of the metal with the electron-electron interaction the diffuse correction to the conductivity

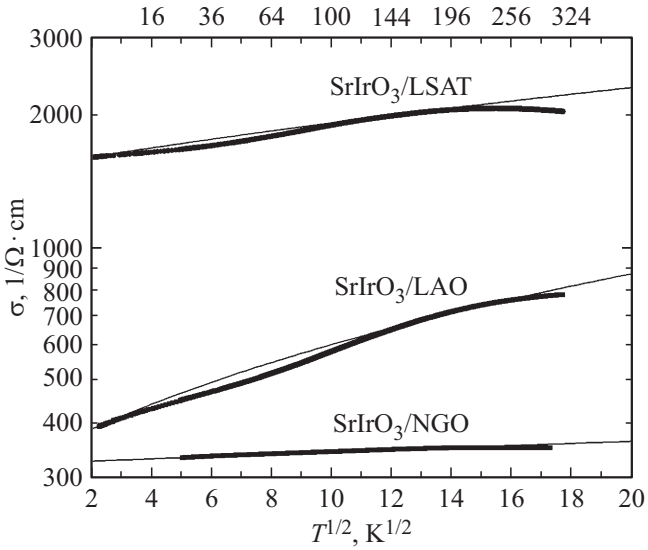

Figure 1. Temperature dependences of conductivities of epitaxial $SrIrO_3$ films on substrates: LSAT at thickness of $t = 90$ nm, at LAO — at $t = 90$ nm, at NGO — at $t = 35$ nm are shown with points. Approximations of type $\sigma \sim T^{1/2}$ — are solid lines.

is growing together with temperature [18]:

$$\Delta\sigma = \frac{e^2}{4\pi^2\hbar^2}\left(\frac{4}{d} + 1.5\lambda_\sigma\right)\left(\frac{T}{D}\right)^{d/2-1} \sim T^{1/2}, \qquad (1)$$

where size is $d = 3$ for the case of 3D conductivity, D — carrier diffusion constant, λ_σ — carrier sputtering amplitude. Approximations of temperature dependences of conductivities using formula (1) are shown in Figure 1.

Sr_2IrO_4 films were applied by three methods: sputtering at direct current (DC), impulse voltage (PULSE), laser ablation (PLD) onto the NGO substrate [14]. Figure 2, *a*. shows dependences $\sigma(T)$ of the Sr_2IrO_4 films we produced. The prevalent mechanisms of Sr_2IrO_4conductivity depend on the thickness of films t and temperature T. The following was observed: i) 3D hopping conductivity with the variable range hopping (VRH) and charge carrier localization radii $\alpha \sim 0.3$ nm, ii) thermal activation of charge carriers with the activation energy $\Delta E \sim 0.1$ eV [19]. Figure 2, *b* shows approximations in the VRH model using formulas [19]:

$$\sigma(T) = \sigma_0 \exp\left[-\left(\frac{T_0}{T}\right)^{1/4}\right];\ T_0 = \frac{\beta}{\mathrm{k}g(\mu)\alpha^3}, \qquad (2)$$

where T_0 — constant determined from the experiment, $g(\mu)$ — density of states at Fermi level, α — localization radius, β — coefficient, k — Boltzmann's constant.

The VRH mechanism prevails at temperatures $T > T_{\mathrm{VRH}}$, at the hop radius of less than thickness $r < t$. The radius drops with the temperature growth as $r \sim \alpha(T_0/T)^{1/4}$. We assessed the radii of charge carrier localization with the ratio of $\alpha \sim t(T_{\mathrm{VRH}}/T_0)^{1/4}$. The parameters of the films Sr_2IrO_4 that we obtained are shown in table.

Note that we used NGO substrates coated with the film of $YBa_2Cu_3O_7$ superconductor and then with the strontium

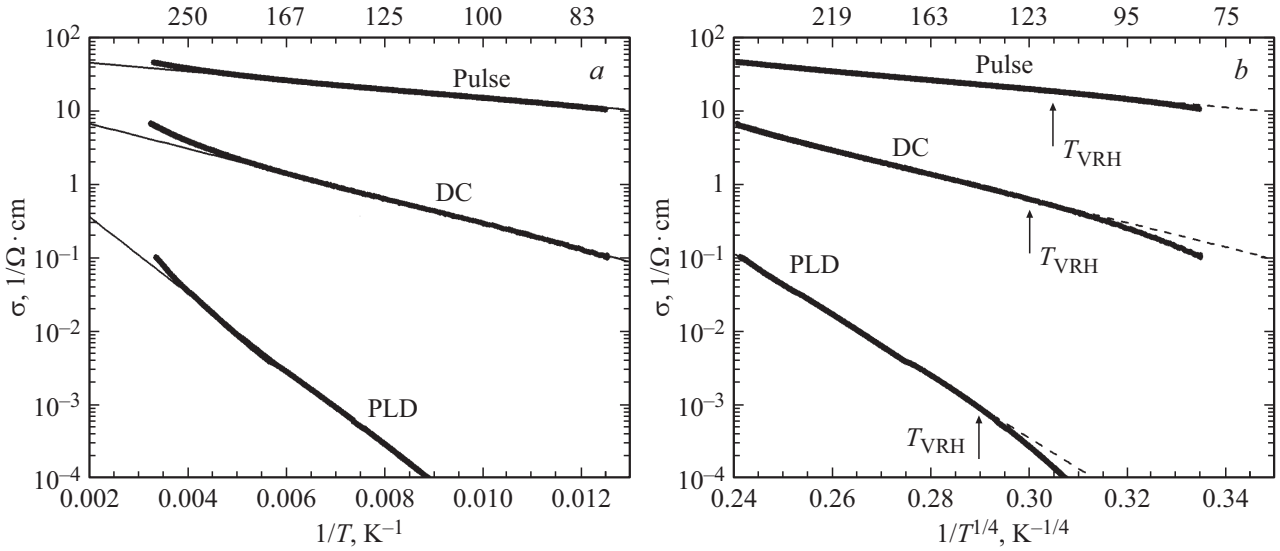

Figure 2. Dependences $\sigma(T)$ for Sr_2IrO_4 films on NGO substrates produced by laser ablation — PLD, sputtering at direct current — DC, voltage pulses — PULSE: *a* — dependences of the reciprocal temperature $1/T$ and *b* — on the reciprocal temperature to the degree of $1/T^{1/4}$, where arrows — are temperatures T_{VRH}.

Parameters of epitaxial Sr_2IrO_4 films in model VHR

Samples	Thickness t, nm	Density of states $g(\mu)$, $eV^{-1}\,cm^{-3}$	Radius α, nm
PLD	35	$1 \cdot 10^{17}$	1–1.5
DC	15	$3 \cdot 10^{18}$	1–1.5
PULSE]	40	$3 \cdot 10^{17}$	9–12
Dependence R_N on thicknesses of barriers, [13]	5–7	–	1.2–1.7

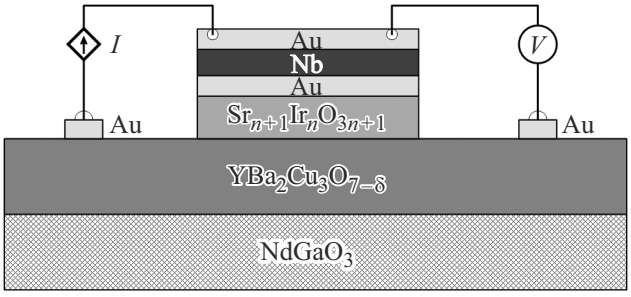

Figure 3. Image of the superconducting heterostructure with SI and electrical leads to measure CVC. Thickness of $YBa_2Cu_3O_{7-\delta}$ $t_{YBCO} = 60–70$ nm, Nb $t_{Nb} = 200$ nm, thin layer of Au under Nb $t_{Au} = 10–20$ nm (more than 5 times less than the free path length in gold) in layer $SrIrO_3$ $t = 14$ nm, for Sr_2IrO_4 $t = 5$ nm.

iridate layer to make the superconducting heterostructures. The PLD sputtering method was used.

4. Electrophysical properties of mesa-heterostructures

Figure 3 shows the layer-by-layer image of a superconducting mesa-heterostructure (MHS) with strontium iridate layers.

The superconducting Au/Nb bilayer had critical temperature $T_C = 8.4$ K, which defines the temperature of transition to the superconducting state of the entire MHS. MHS of two types $Nb/Au/Sr_2IrO_4/YBa_2Cu_3O_7$ and $Nb/Au/SrIrO_3/YBa_2Cu_3O_7$ were made and studied. A chip 5×5 mm was used to make 5 MHSs with planar dimensions from $10 \times 10\,\mu m^2$ to $50 \times 50\,\mu m^2$. Supercurrent was observed in both types of MHS. Temperature dependence of critical current $I_C(T)$ followed the temperature dependence of Nb gap [10].

Figure 4, *a* shows the magnetic-field dependence of critical current $I_C(H)$ and CVC for MHS with SI layer $SrIrO_3$ for the case of $t = 14$ nm and the size of $50 \times 50\,\mu$m. You can see that the experimental dependence $I_C(H)$ has a more pronounced central maximum and zero minima, which is typical for Fraunhofer dependence$I_C(H) \sim abs[\sin(\pi HA)/(\pi HA)]$, for the concentrated Josephson junctions [20]. Figure 4, *b* shows 4 CVCs of MHS with SI layer with thickness of $t = 14$ nm.

Due to a small difference between the superconducting critical current j_C of MHS in the unpairing current density j_S for the supplying superconducting electrodes, CVCs demonstrated bends at $I > 300\,\mu$A (Figure 4, *b*), therefore the value R_N was defined by inclination of the resistive area. From Figure 4, *b* you can see that CVCs *1* and *2* at $I = 0$ cross the $V = 0$ and practically overlap at $I > 300\,\mu$A due to pair breaking of the superconducting electrodes. For MHs with $SrIrO_3$ layers the average current density $j_C = 5–10$ A/cm^2, resistance $R_N A = (3–5) \cdot 10^{-8}\,\Omega\,cm^2$.

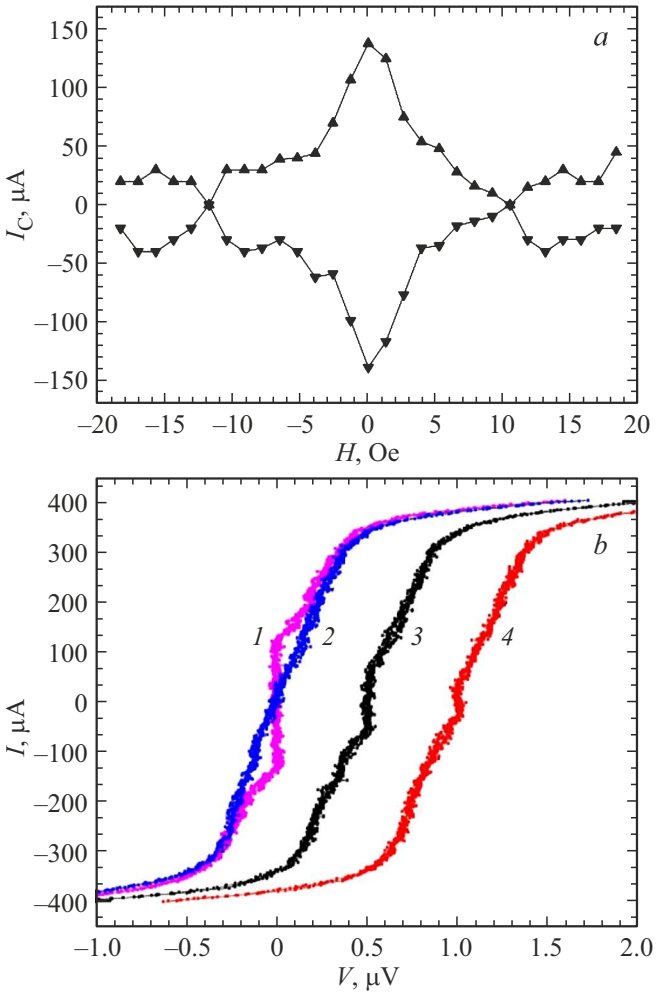

Figure 4. *a* — dependence $I_C(H)$ at $T = 4.2$ K for heterostructure with layer of $SrIrO_3$ $t = 14$ nm, $L = 50\,\mu$m. *b* — CVC series, the numbers comply with the following: *1* — $H = 0$, *2* — $H = 10$ Oe, *3* — $H = 2.5$ Oe, *4* — $H = 14.5$ Oe. Curves *3* and *4* are displaced along the x axis relative to $V = 0$.

Let us discuss the experimental CVCs of MHS $Nb/Au/Sr_2IrO_4/YBa_2Cu_3O_x$ with thickness of SI layer Sr_2IrO_4 $t = 5$ nm and size of $L = 40 \times 40\,\mu$m. Figure 5, *a* shows the magnetic-field dependence of the critical current $I_C(H)$, obtained from CVC family, some of them are shown in Figure 5, *b*. CVCs were plotted in the mode of current setting using 4-point measurement layout. The magnetic field parallel to the substrate plane was set by the solenoid located inside the hollow screen made of multi-layer amorphous permalloy that reduces the geomagnetic field by an order. The calculated value using Fraunhofer dependence $I_C(H)$ yields the first minimum value $H_1 = \Phi_0/\Lambda L \simeq 2$ Oe at $\lambda_{L1} = 150$ nm for $YBa_2Cu_3O_x$ and $\lambda_{L2} = 90$ nm for Nb, even thought the shape of the experimental dependence $I_C(H)$ in Figure 5, *a* differs from the Fraunhofer's one. There was asymmetry of CVC shape that manifested itself both in the difference of „positive“ and „negative“ amplitudes of critical current relative to $I = 0$, and in the occurrence of wave-like features seen well in the curves *1*–*3* in Figure 5, *b*. At $H \neq 0$, following the analogy with the tunnel SIS (superconductor-isolator-superconductor) junctions, wave-like features are explained by Fiske resonant cavities [21,22], and at $H = 0$ by the impact of „internal“ magnetic field due to SOI layer Sr_2IrO_4 [11,12]. Fiske steps at a SIS junction arise at voltages $V_n = n\Phi_0 c/2L$, where n-number of the step, Φ_0 — magnetic flux quantum) $c = c(t/\varepsilon\Lambda)^{1/2}$ — Swihart speed [23], c — speed of light in vacuum, L — junction width, t — thickness of isolator layer with dielectric permeability ε, Λ — depth of magnetic field penetration.

In case of SI_FS tunnel junction with magnetic isolator I_F, the depth of magnetic field penetration is $\Lambda = \mu t + \lambda_{L1}\,\mathrm{cth}(d_1/2\lambda_{L1}) + \lambda_{L2}\,\mathrm{cth}(d_2/2\lambda_{L2})$, where μ — magnetic permeability, $d_{1,2}$ and $\lambda_{L1,2}$ — thicknesses of superconducting films and their London depths of magnetic field penetration accordingly. Based on the absence

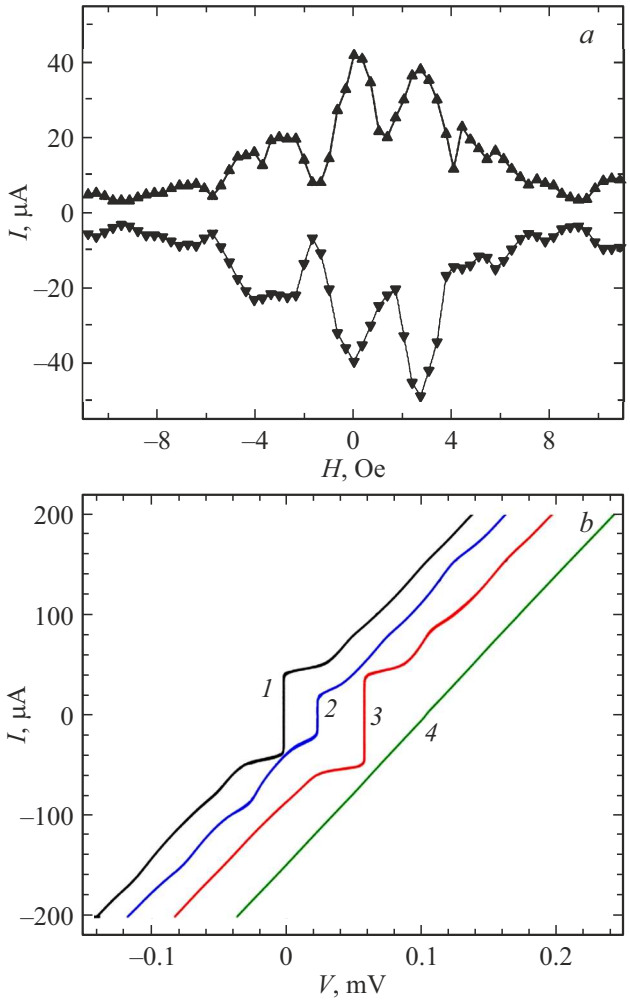

Figure 5. *a* — dependence $I_C(H)$ for a heterostructure with Sr_2IrO_4 layer $t = 5$ nm, $L = 40\,\mu$m. *b* — CVC series, for magnetic field: *1* — $H = 0$, *2* — $H = +2.7$ Oe, *3* — $H = -2.5$ Oe, *4* — $H = -9.6$ Oe. The change in the sign of the magnetic field corresponds to the change of current direction in the coil. Curves are displaced along the x axis.

of deviated characteristics $I(V)$ by linear dependence at $V > 2\,\text{mV}$ for all CVCs (Figure 5, *b*), first — no excessive current flowing through the structure, second — exposure to electromagnetic irradiation led to Shapiro steps oscillating with the irradiation capacity [12]. These two features of CVCs indicate the absence of short-circuiting jumpers in the structures.

5. Conclusion

The experimental data on temperature characteristics led to establishment of the current carrier transport mechanisms in thin films of strontium iridate with strong spin-orbit interaction produced by three technological methods: by sputtering at direct current, using a pulse source of voltage and laser ablation. The superconducting mesa-heterostructures were made and studied with the two types of the layer of strontium iridate — with the conducting $SrIrO_3$ and dielectric antiferromagnetic Sr_2IrO_4. Both types of heterostructures demonstrated the Josephson effect.

Funding

The research was supported by a grant from the Russian Science Foundation No. 23-49-10006, https://rscf.ru/project/23-49-10006/

Conflict of interest

The authors declare that they have no conflict of interest.

References

[1] M. Eschrig. Rep. Prog. Phys. **78**, 104501 (2015). DOI: 10.1088/0034-4885/78/10/104501
[2] J. Linder, J.W.A. Robinson. Nat. Phys. **11**, 307 (2015). DOI: https://doi.org/10.1038/nphys3242
[3] M. Horsdal, G. Khaliullin, T. Hyart, B. Rosenow. Phys. Rev. B **93**, 220502(R) (2016). DOI: 10.1103/PhysRevB.93.220502
[4] F.S. Bergeret, I.V. Tokatly. Phys. Rev. B **89**, 134517 (2014). DOI: 10.1103/PhysRevB.89.134517
[5] S.H. Jacobsen, J. Linder. Phys. Rev. B **92**, 024501 (2015). DOI: 10.1103/PhysRevB.92.024501
[6] F. Konschelle, I.V. Tokatly, F.S. Bergeret. Eur. Phys. J. B **87**, 119 (2014). DOI: 10.1140/epjb/e2014-50143-0
[7] N. Satchell, N.O. Birge. Phys. Rev. B **97**, 214509 (2018). DOI: 10.1103/PhysRevB.97.214509
[8] G. Cao, P. Schlottmann. Rep. Progress in Phys. **81**, 042502 (2018). DOI: 10.1088/1361-6633/aaa979
[9] Yige Chen, Hae-Young Kee. Physical Rev. B **97**, 085155 (2018). DOI: 10.1103/PhysRevB.97.085155
[10] A.M. Petrzhik, K.Y. Constantinian, G.A. Ovsyannikov, A.V. Zaitsev, A.V. Shadrin, A.S. Grishin, Yu.V. Kislinskii, G. Cristiani, G. Logvenov. Phys. Rev. B **100**, 024501 (2019). DOI: 10.1103/PhysRevB.100.024501
[11] K.Y. Constantinian, A.M. Petrzhik, G.A. Ovsyannikov, A.V. Shadrin, Yu.V. Kislinskii, G. Cristiani, G. Logvenov. Journal of Physics Conference Series **1559**, 012023 (2020). DOI: 10.1088/1742-6596/1559/1/012023
[12] K.Y. Constantinian, G.A. Ovsyannikov, A.M. Petrzhik, A.V. Shadrin, Yu.V. Kislinskii, G. Cristiani, G. Logvenov. Physics of the Solid State **62**, *9*, 1549 (2020). DOI: 10.1134/S1063783420090152
[13] Y.V. Kislinskii, K.Y. Constantinian, I.E. Moskal, N.V. Dubitskiy, A.M. Petrzhik, A.V. Shadrin, G.A. Ovsyannikov. Russian Microelectronics **52**, S53 (2023). DOI: 10.1134/S1063739723600802
[14] Yu.V. Kislinskii, K.Y. Constantinian, I.E. Moskal, A.M. Petrzhik, A.V. Shadrin, G.A. Ovsyannikov. Physics of the Solid State **64**, *10*, 1394 (2022).
[15] A. Biswas, K.S. Kim, Y.H. Jeongl. Journal of Appl. Phys. **116**, 213704 (2014). http://dx.doi.org/10.1063/1.4903314
[16] M.K. Crawford, M.A. Subramanian, R.L. Harlow. Phys. Rev. B **49**, 9198 (1994).
[17] N.E. Hussey, K. Takenaka, H. Takagi. Philosophical Magazine **84**, 2847 (2004). http://dx.doi.org/10.1080/14786430410001716944
[18] B.L. Altshuler, A.G. Aronov. Electron–Electron Interactions In Disordered Conductors. In the book Electron–Electron Interactions in Disordered Systems. Eds by A.J. Efros, M. Pollack. De Gruyter, Amsterdam, North Holland (1986). https://doi.org/10.1515/9783112494721-070
[19] Chengliang Lu, Andy Quindeau, Hakan Deniz, D. Preziosi, D. Hesse, M. Alexe. Appl. Phys. Lett. **105**, 082407 (2014). http://dx.doi.org/10.1063/1.4894465
[20] A. Barone, G. Paterno. Physics and Applications of the Josephson Effect, Wiley (1982).
[21] D.D. Coon, M.D. Fiske. Phys. Rev. **138**, A744 (1965).
[22] I.O. Kulik. Pisma v ZhETF **2**, 134 (1965). (in Russian).
[23] J.C. Swihart. J. Appl. Phys. **32**, 461 (1961). https://doi.org/10.1063/1.1736025

Translated by M.Verenikina